SOD2 in Skeletal Muscle: New Insights from an Inducible Deletion Model.

Aowen Zhuang[1,2,3], Christine Yang[1], Yingying Liu[1], Yanie Tan[1,2] Simon T. Bond[1,2,3], Shannen Walker[1,2], Tim Sikora[1], Arpeeta Sharma[1], Judy B. de Haan[1,2,3,4,5], Peter J. Meikle[1,2,3], Melinda T. Coughlan[1,6], Anna C. Calkin[1,2,3] & Brian G. Drew[1,2,3]*

1. Baker Heart & Diabetes Institute, Melbourne, Australia, 3004.
2. Central Clinical School, Monash University, Melbourne, Australia, 3004
3. Baker Department of Cardiometabolic Health, University of Melbourne, Melbourne, Australia,
4. Department of Physiology, Anatomy and Microbiology, La Trobe University, Melbourne, Australia, 3083
5. Faculty of Science, Engineering and Technology, Swinburne University, Melbourne, Australia, 3122
6. Department of Diabetes, Central Clinical School, Monash University, Melbourne, Australia, 3004

* Author for correspondence: brian.drew@baker.edu.au

Abstract

Metabolic conditions such as obesity, insulin resistance and glucose intolerance are frequently associated with impairments in skeletal muscle function and metabolism. This is often linked to dysregulation of homeostatic pathways including an increase in reactive oxygen species (ROS) and oxidative stress. One of the main sites of ROS production is the mitochondria, where the flux of substrates through the electron transport chain (ETC) can result in the generation of oxygen free radicals. Fortunately, several mechanisms exist to buffer bursts of intracellular ROS and peroxide production, including the enzymes Catalase, Glutathione Peroxidase and Superoxide Dismutase (SOD). Of the latter there are two intracellular isoforms; SOD1 which is mostly cytoplasmic, and SOD2 which is found exclusively in the mitochondria. Developmental and chronic loss of these enzymes has been linked to disease in several studies, however the temporal effects of these disturbances remain largely unexplored. Here, we induced a post-developmental (8-week old mice) deletion of SOD2 in skeletal muscle (SOD2-iMKO) and demonstrate that 16 weeks of SOD2 deletion leads to no major impairment in whole body metabolism, despite these mice displaying alterations in aspects of mitochondrial abundance and voluntary ambulatory movement. Furthermore, we demonstrated that SOD2 deletion impacts on specific aspects of muscle lipid metabolism, including the abundance of phospholipids and phosphatidic acid (PA), the latter being a key intermediate in several cellular signaling pathways. Thus, our findings suggest that post-developmental deletion of SOD2 induces a more subtle phenotype than previous embryonic models have shown, allowing us to highlight a previously unrecognized link between SOD2, mitochondrial function and bioactive lipid species including PA.

Introduction

Insulin resistance, glucose intolerance and type 2 diabetes are strongly influenced by a combination of genetics and lifestyle, which is further compounded by the process of ageing[1]. Many pathways have been identified as contributing determinants of these diseases, however one of the most consistent, reproducible features amongst them all is mitochondrial dysfunction[2]. This suggests a direct association between mitochondrial function in peripheral tissues and the progression of metabolic disease, however which of these conditions is the primary driving factor remains to be determined. In an effort to tease out this relationship, studies have suggested that early insults that directly impact on mitochondria, such as mutations in key mitochondrial genes, promote mitochondrial dysfunction and induce type 2 diabetes[3].

When mitochondria are dysfunctional they are often less efficient at generating ATP through oxidative phosphorylation, and thus several toxic by-products are generated including excessive amounts reactive oxygen species (ROS). Whilst ROS in normal concentrations are important cellular signaling molecules, excessive and chronic production of ROS can lead to deleterious effects including oxidation of proteins and metabolites, mutation of mitochondrial DNA, inhibition of glycolysis and the promotion of advanced glycation end products[4]. Fortunately, in a healthy cell several mechanisms exist to buffer these transient bursts of ROS, including the activity of intracellular enzymes such as Catalase and Glutathione Peroxidase (Gpx1), and two isoforms of Superoxide Dismutase (SOD); SOD1 and SOD2[5].

The ROS buffering capacity of a cell can, however, be significantly reduced by several mechanisms including mutations in genes important for ROS production or scavenging, or perturbations to energy substrate metabolism. For example, when a cell is exposed to high

3

71   levels of glucose, this forces excess substrate through the electron transport chain (ETC),

72   placing a greater demand on resources[4]. Inevitably, the ETC becomes overloaded and unless

73   there is an outlet for the increased electrons produced along the pathway such as uncoupling

74   proteins, they are instead shunted onto molecular oxygen which chemically reduces it to

75   produce superoxides, or ROS. This increase in ROS further reduces mitochondrial capacity

76   and thus sets in place a vicious cycle whereby increasing glucose concentrations continues to

77   elevate levels of ROS, and vice versa[5].

78

79   Depending on the tissue in which mitochondrial dysfunction and chronic ROS accumulation

80   occurs, it can manifest in different phenotypes. Chronic increases in ROS promotes

81   cardiomyopathy, chronic kidney disease and skeletal muscle atrophy and perturbed energy

82   metabolism[6]. All of these phenotypes are common in the setting of glucose intolerance and

83   diabetes, suggesting that prevention or treatment of pathways that lead to elevated ROS, is of

84   potential therapeutic interest.

85

86   Many groups have been interested in the notion that reducing excessive ROS is a means to

87   preventing disease. Indeed, several pharmaceutical companies have made significant

88   investments into developing modified antioxidant molecules such as MitoQ, MTP-131 and

89   SkQ1 that have demonstrated various levels of efficacy in human trials of sarcopenia, cardiac

90   disease and fatty liver disease[7]. Moreover, preclinical genetic models have elegantly

91   demonstrated that global overexpression of antioxidant enzymes such as catalase and SOD,

92   which aid in mopping up excess ROS, have efficacy in preventing endothelial dysfunction,

93   atherosclerosis, fatty liver, heart disease and glucose intolerance[8,9]. On the contrary, global

94   genetic deletion of these enzymes induce pathological phenotypes. For example, homozygous

95   deletion of SOD2 (Mn-SOD), a variant of SOD found exclusively in the mitochondria, led to

4

96   neonatal lethality[10]. Furthermore, although viable, heterozygous SOD2 mutants present with

97   many pathologies consistent with mitochondrial dysfunction including poor tolerance to

98   exercise, cardiomyopathy, cardiovascular disease and glucose intolerance[9,11-15]. Thus,

99   manipulating cellular ROS either through pharmacological or genetic means appears to

100   impact on disease outcomes. A potential downside with the majority of studies thus far, has

101   been the inability to tease out what the tissue specific effects of ROS damage are, which

102   might aid in improving antioxidant targeting for therapeutic benefit.

103

104   One enzyme studied for its tissue specific effects is SOD2, with liver[16], brain[17], adipose[18],

105   heart[19], smooth muscle[20] and skeletal muscle[14,15] specific models all having been generated

106   and phenotyped. Interestingly, the skeletal muscle specific studies have demonstrated striking

107   defects in exercise capacity, muscle strength and mitochondrial activity, similar to what has

108   been observed in whole body models[14,15]. An important point to note is that these prior

109   models deleted SOD2 during early development, raising questions as to whether the observed

110   phenotypes were due to increased mitochondrial ROS in fully matured muscle *per se*, or

111   whether in fact the loss of SOD2 and a subsequent increase in ROS in the developmental

112   stages, impacted skeletal muscle development directly. Thus, studies which aim to understand

113   the effect of SOD2 deletion in skeletal muscle post-development, stand to overcome this

114   limitation and shed new light on our understanding of this pathway.

115

116   In this study we investigated the molecular and metabolic effects of SOD2 deletion from the

117   musculature in post-developmental male mice from 8 weeks of age.

118   **Results**

119   **Generation and validation of post-developmental, skeletal muscle specific SOD2-knock**

120   **out mice**

121   To generate mice with deletion of SOD2 in skeletal muscle post-development, we crossed

122   SOD2 floxed (SOD2 fl/fl) mice with ACTA1-creERT2 (mCre) mice. The resulting SOD2

123   fl/fl and fl/fl-creERT2 (fl/fl-mCre) male mice were subsequently administered Tamoxifen

124   (TAM; 80mg/kg) in sunflower oil treated by gavage, or with sunflower oil alone for 3

125   consecutive days at approximately 8 weeks of age to activate cre-recombinase. Mice were

126   then fed a high fat diet for the subsequent 12 weeks to metabolically stress the animals. A

127   separate cohort of fl/fl and fl/fl-mCre mice were treated with tamoxifen, and fed a normal

128   chow diet for 12 weeks (no vehicle control mice for chow study). High fat diet (HFD) mice

129   underwent a comprehensive phenotyping regimen over the 12-week period before collecting

130   tissues at the end of the study following a 6 hour fast. Blood and tissues were also collected

131   from chow fed mice at study end.

132

133   Using qPCR analysis (see **Table 1** for qPCR primers sets) on muscle acquired from HFD fed

134   mice, we demonstrated that cre-recombinase expression was specific to skeletal muscle, with

135   no expression detected in liver or white adipose tissue (WAT) (**Figure 1A**). Moreover, SOD2

136   mRNA expression was almost completely ablated in skeletal muscle, whereas no change was

137   observed in liver or WAT (**Figure 1B**). To investigate the effect of cre-lox activity in

138   different muscle tissues, we investigated cre-recombinase and SOD2 mRNA expression in a

139   mixed fibre-type muscle (*Tibialis anterior* – TA), a red fibre-type muscle (*soleus*) and a

140   white fibre-type muscle (*Extensor digitorum longus* – EDL). These results demonstrate that

141   cre-expression appears to be lower in the *Soleus* red muscle fibre type compared to TA and

142   EDL (**Figure 1C**), however the deletion of SOD2 was equivalent between all three muscle

6

143   types (**Figure 1D**), validating SOD2-deletion in all muscle types. To confirm that ablation of

144   SOD2 mRNA resulted in deletion of the SOD2 protein, we performed western blots on TA

145   muscles from both chow and high-fat diet (HFD) fed mice. This demonstrated almost

146   complete ablation of SOD2 in fl/fl-mCre (KO) muscle compared to fl/fl mice (WT) (**Figure**

147   **1E**).

148

149   Upon demonstrating that SOD2 mRNA and protein was specifically deleted in the skeletal

150   muscles of fl/fl-mCre mice, we next sought to investigate the effect of SOD2 deletion on

151   readouts of redox regulation in skeletal muscle. This was performed on three different

152   muscles (TA, EDL and Soleus) from HFD fed animals, across all 4 groups of mice;

153   WT+OIL, mCre+OIL, WT+TAM and mCre+TAM. We initially performed gene expression

154   analysis using qPCR for known enzymes that are involved in redox regulation including *Nrf2*,

155   *p47Phox*, *p22Phox* and *Nox2* (**Figures 1F-H**)**.** These genes were largely unaffected by the

156   deletion of SOD2 (dark blue bars), except for *Nox2* which was significantly increased in TA

157   of KO mice (**Figure 1H, dark blue bar**), whilst *Nrf2* and *p47phox* showed a trend to be

158   increased in the EDL of KO mice (**Figure 1G, dark blue bar**). No genes were altered by the

159   deletion of SOD2 in the soleus, although it did appear that Tamoxifen treatment alone

160   induced a general reduction in each of the genes assayed (**Figure 1H**, blue bars).

161

162   Next we investigated the effect of SOD2 deletion on the abundance of reactive oxygen

163   species (ROS), and downstream products known to be altered by oxidative stress. **Figure 1I**

164   shows the abundance of 4-hydroxynonenal (4HNE) protein adducts as determined by

165   Western blot, which are often generated as a result of increased free radicals. Skeletal muscle

166   deletion of SOD2 resulted in a reduction of 4HNE staining in TA muscles from both chow

167   and HFD fed animals, which was significantly ($p=0.004$) different in the HFD fed animals

168   (**Figure 1J**), indicating a reduced protein peroxidation in the absence of SOD2. We also

169   performed a direct measure of peroxides (e.g. H_2O_2) in the TA muscles using an Amplex Red

170   Assay, which demonstrated an increase in the abundance of peroxides in the skeletal muscle

171   of HFD fed animals compared to chow fed animals. However, SOD2 KO did not have any

172   impact on peroxide abundance (**Figure 1K**), which is somewhat surprising given that the role

173   of SOD2 is to convert mitochondrial superoxides and thus one might have expected a

174   decrease in peroxide concentration in the absence of SOD2. Given there was no change in the

175   level of peroxide in SOD2 KO compared to WT HFD fed mice, this would suggest that the

176   majority of peroxide generated in this setting are not derived from the mitochondria, and is

177   likely impacted by alterations in other enzymes including SOD1. Finally, we measured the

178   amount of nitrotyrosine products generated in TA muscles of WT and SOD2-KO (mCre)

179   HFD fed mice. This demonstrated a ~2-fold increase in positive staining for nitrotyrosine in

180   muscle sections of SOD2 KO muscle ($p<0.05$; **Figure 1L**), suggestive of increased

181   superoxide levels in SOD2 KO that lead to increased protein nitration via peroxynitrite

182   intermediates. Together, these data confirm that post-developmental deletion of SOD2 leads

183   to alterations in redox readouts in skeletal muscle, with nitrotyrosine noticeably increased in

184   KO muscles.

185

186   **Inducible, muscle specific knock out of SOD2 has no effect on body mass or organ**

187   **weights**

188   Upon demonstrating successful generation of muscle specific SOD2 KO mice with mild

189   alterations to redox homeostasis, we sought to investigate if feeding these mice a HFD led to

190   genotype specific alterations in body mass and tissue weights. Weekly analysis of body

191   weight revealed that KO mice (mCre+TAM) had a similar weight gain over the 12 week

192   study compared to the three control models (WT+OIL, mCre+OIL, WT+TAM) (**Figure 2A**).

193   This was confirmed by EchoMRI that demonstrated no difference in lean mass (**Figure 2B**)

194   or fat mass (**Figure 2C**) between all groups at any of the timepoints measured; however, it

195   did demonstrate marked increase in fat mass in all models in response to HFD, as expected.

196   With regard to organ weights at study end, we demonstrated no difference in EDL (**Figure**

197   **2D**), TA (**Figure 2E**), liver (**Figure 2F**) or gonadal white adipose tissue (gWAT) (**Figure**

198   **2G**) weight across the four cohorts. Overall, these data demonstrated that inducible, muscle

199   specific SOD2 KO does not alter body mass or tissue weights in mice fed a HFD for 12

200   weeks.

201

202   **Inducible, muscle specific knock out of SOD2 alters ambulatory movement behaviour,**

203   **but does not affect glucose tolerance**

204   After demonstrating that inducible deletion of SOD2 in skeletal muscle had no effect on total

205   body mass or organ weights, we sought to determine if subclinical changes in metabolism

206   and movement behavior were apparent in these mice. To study these outputs, we placed the

207   WT+TAM and mCre+TAM cohorts in a Promethion High-Definition Multiplexed

208   Respirometry System both prior to commencement of diet (baseline) and after 10 weeks of

209   HFD feeding (End HFD). The Promethion system performs repeated measures of whole body

210   respiration, activity behavior and daily movement of individual mice across the entire 24-

211   hour analysis period. These studies demonstrated that the respiratory exchange ratio (RER)

212   between the two genotypes was not different at any particular period over the 24 hours

213   (**Figure 3A**). There was also no difference in RER between genotypes at baseline or after

214   HFD (**Figures 3B&3C**), or in energy expenditure (EE) (**Figures 3D&3E**). However, as

215   expected there was a drop in the RER observed between baseline and HFD, particularly

216   during the night period (~0.85 to 0.78 at light, ~0.93 to 0.6 at dark, for NC vs HFD

217   respectively), consistent with the animals using more fat for energy production. HFD feeding

218   also coincided with an increased EE after HFD feeding compared to baseline, which was

219   particularly noticeable during the light cycle, likely reflecting the high-energy content of the

220   diet they were consuming.

221

222   Further to respiration and energy expenditure measures, the Promethion system is able to

223   provide insights into animal behavior and ambulatory movement. We observed a noticeable

224   shift in the times and pattern of active movement in the KO mice compared to WT mice

225   (**Figure 3F**). In this panel, it was observed that KO animals tended to do more intense

226   movement early on in the night cycle, when they first wake, compared to WT mice.

227   Following this bout of movement, they tended not to move again substantially until the end of

228   the night cycle, which then continued well into the early part of the day cycle. These altered

229   behaviors encouraged us to investigate this finding further, and thus we studied their

230   locomotion and exercise behaviours. To do this we compared the distance and speed at which

231   they travelled on the running wheel at the start of the study (baseline), with that at the end of

232   the study (end of HFD). This was performed for both genotypes and separated into light and

233   dark activity cycles. Thus, if the distance and speed the mice covered was the same at the

234   beginning and the end of the study, the "delta" would be zero. We demonstrated that there

235   was no difference in the distance both genotypes ran at the start and the end of study during

236   the day time cycle (**Figure 3G**), nor was there a difference in WT mice in the night time

237   cycle. However, there was a strong trend for a reduced distance covered by KO mice in wheel

238   distance in the night time cycle, as indicated by the negative delta. With regards to wheel

239   speed, we demonstrated that both genotypes were unable to maintain the same speed at the

240   end of the study compared to their baseline speeds (perhaps due to the HFD), however there

241   was a noticeable and robust decline in wheel speed in the KO mice in the nighttime cycle

10

242 compared to WT mice (**Figure 3H**). These data collectively demonstrate that KO mice have a

243 decline in the capacity to travel the same distance, and at the same speed as WT mice.

244

245 Another measure we can obtain from Promethion is positional probability mapping, which

246 uses data collected over the entire analysis period to estimate cumulative animal movement

247 behaviours. This analysis demonstrated that KO mice spend more time "lounging" in specific

248 regions of the cage for long periods of time than WT mice (**Figure 3I and 3J**). This can be

249 observed both in the day time (**Figure 3I**), where less lounge spots for the KO mice indicate

250 longer time spent in the one spot, and at night time (**Figure 3J)** where the KO mice spend far

251 less time near the wheel and closer to lounge spots. In an attempt to quantify these

252 observations, we used behavioral transition analysis to infer the percent of time the different

253 genotypes spent doing each activity (**Figure 3K&3L**). The propensity for KO mice to take a

254 long lounge (llnge) appeared to be more apparent after they had either eaten food, drank

255 water or undertaken exercise (KO vs WT: 41% vs 26%, 36% vs 25%, 59% vs 24%

256 respectively), suggestive of fatigue (increased percentage shown in red). Indeed, WT mice

257 were more likely to take a short lounge (slnge) after eating or drinking, supporting the notion

258 that KO mice were more lethargic and less willing to stay active after these activities.

259

260 To determine whether these alterations in ambulatory movement and animal behavior

261 impacted on metabolism of energy substrates in these mice, we assessed their whole body

262 glucose regulation. At baseline there were no differences in either basal fasting glucose

263 (**Figure 3M**), or in their tolerance to a standardized bolus of glucose (**Figure 3N**). Indeed,

264 this remained similar throughout the HFD feeding regimen where, despite glucose tolerance

265 deteriorating as expected over the HFD feeding period, it remained similar between the KOs

266 and all three control models at both 4 weeks and 12 weeks post diet (**Figures 3O-3R**). Thus,

267   although the movement and behavior of the KO mice was altered, this did not appear to

268   impact on glucose tolerance in these animals, even following a 12-week HFD challenge.

269

270   **Inducible, muscle specific knock out of SOD2 induces changes in skeletal muscle**

271   **mitochondrial composition**

272   Given that SOD2 is localized to the mitochondria, and that we observed phenotypes in KO

273   mice that were reminiscent of lethargy that is often observed in models with mitochondrial

274   deficits, we performed experiments to test aspects of mitochondrial activity. We initially

275   performed analysis on the abundance of mtDNA in the TA muscle of all four cohorts from

276   the HFD study (**Figure 4A**). These data demonstrated that mtDNA abundance was not

277   different between KO mice and the various control cohorts. Next, we performed Western blot

278   analysis on the TA muscles from WT+TAM and mCre+TAM animals fed both chow and

279   HFD to investigate the abundance of representative proteins from each of the five complexes

280   of the electron transport chain (ETC) (**Figure 4B**). These data demonstrated that SOD2 KO

281   mice had a substantial reduction in the abundance of both Complex I and Complex II proteins

282   of the ETC (**Figure 4C**). Moreover, although not significant, there was a notable trend for a

283   reduction in all other complexes of the ETC. Given the robust reductions in ETC complex I

284   and II, we performed gene expression analysis on the three different muscle types (TA, EDL,

285   Soleus) from all four cohorts of mice that were fed a HFD, to determine if this phenotype

286   might be driven by transcriptional changes in mitochondrial genes (**Figures 4D-4F**). These

287   data demonstrated that although some genes were modestly changed in KO TA muscles (e.g.

288   *Ppargc1a* and *Ndufs1*), overall the expression of key mitochondrial genes was not altered by

289   deletion of SOD2. These findings indicated that key components of the mitochondrial ETC

290   were reduced in SOD2 KO skeletal muscles, but this was not due to changes in mtDNA

291   abundance or changes in gene transcription, suggesting a post-translational effect on ETC

292   complex abundance in this model potentially due to altered redox homeostasis.

293

294   **Inducible, muscle specific knock out of SOD2 alters pathways involved in energy**

295   **substrate utilisation.**

296   Given the subtle alterations in mitochondrial readouts, we speculated whether SOD2 KO

297   mice might also demonstrate changes in pathways that regulate skeletal muscle energy

298   metabolism. A well-described regulator of skeletal muscle energy metabolism is AMP

299   activated protein kinase (AMPK), which alters both glucose and lipid metabolism in the

300   setting of increased energy demand. We performed Western blots in the TA muscles from

301   both chow and HFD fed WT and KO mice, which demonstrated that SOD2 KO muscles had

302   an increased phosphorylation of the AMPKalpha subunit at the Thr172 activation site,

303   compared to WT mice (**Figure 5A&5B**). Basal phosphorylation of AMPK was blunted in

304   WT mice fed a HFD, however the increase in AMPK phosphorylation that was observed in

305   KO mice fed a chow diet was abolished in KO mice fed a HFD. This result suggested that

306   loss of SOD2 in a chow setting impacted on metabolic pathways that resulted in an increased

307   need for energy, perhaps due to loss of mitochondrial efficiency, however this effect was

308   confounded by the HFD milieu. In an attempt to further investigate the impact on muscle

309   function, we performed qPCR analysis in the TA, EDL and Soleus muscles. There were no

310   statistically significant differences in the abundance of any metabolism related genes in the

311   KO (mCre+TAM) group compared to the three control groups (**Figure 5B-5D**). Moreover,

312   given previous studies have indicated that developmental loss of SOD2 in skeletal muscle can

313   lead to alterations in muscle morphology and branching [21], we subsequently analyzed the

314   abundance of genes that might suggest changes in these pathways. Our data demonstrated

315   that there was a change in the abundance of *Mef2c*, *Myog* and *Myod*, which are

13

316   transcriptional regulators of skeletal muscle myogenesis (**Figure 5B-5D)**. Specifically, there

317   was a trend towards reduced *Mef2C* and *MyoD* in the TA muscle, and in *MyoD* in the EDL.

318   These findings are consistent with those previously described, and potentially indicate that

319   SOD2 null muscle has a mild impairment in muscle myogenesis.

320

321   **Inducible, muscle specific knock out of SOD2 alters specific lipid pathways in skeletal**

322   **muscle tissue.**

323   Finally, given that we have shown that inducible SOD2 deletion in skeletal muscle leads to

324   subtle changes in mitochondrial and metabolic pathways, we sought to investigate if these

325   changes affected lipid metabolism. Lipids are important signaling molecules, critical

326   substrates for energy metabolism, and potent regulators of mitochondrial function. Thus, we

327   performed ESI-MS/MS lipidomics analysis on muscle homogenates from all four cohorts of

328   mice fed a HFD, and compared their lipidomes. We first analysed the total abundance of each

329   of the 33 classes of lipids, which provided a global insight into the skeletal muscle lipidomes

330   across the cohorts (**Figure 6A**). It was observed that in general the tamoxifen treatment had a

331   noticeable impact on muscle lipid abundance, with an evident reduction in the abundance of

332   several classes in mice treated with tamoxifen. This was particularly apparent in the

333   triglyceride class (TG-SIM and TG-O), where these lipids appeared to be reduced by up to

334   50% as a response to Tamoxifen (WT+TAM and mCre-TAM cohorts; **Figure 6A**). Whilst

335   many of the lipid classes were unaffected by the tamoxifen and deletion of SOD2, there were

336   three particular lipid classes that were significantly reduced by SOD2 deletion, that were

337   independent of any effects of Tamoxifen itself. These were diacylglycerols (DG), free fatty

338   acids   (FFA)   and   lysophospholipids   (lysophosphatidylcholines   -   LPC,

339   lysophosphatidylethanolamines - LPE and lysophosphatidylinositols - LPI). Several

340   phosphate-containing lipid classes also exhibited a trend towards an increase in abundance in

341   the SOD2 KO muscle, including phosphatidic acids (PA), phosphatidylcholines (PCs) and

342   phosphatidylethanolamines (PEs). Given the significant differences observed in the DGs and

343   FFAs, we performed a more in depth analysis of these lipids to investigate the effect of SOD2

344   KO on the individual species within these classes. We observed that several individual

345   species of DG were significantly reduced by SOD2 KO, including many of the high

346   abundance DGs such as those containing 16:χ and 18:χ fatty acids (**Figure 6B**). This was

347   also reflected in the individual species of FFAs, where significant reductions were also

348   observed for 4 different species including the 16:χ and 18:χ fatty acids (**Figure 6C**). The

349   combined change in lysophospholipids demonstrated the global impact that SOD2 KO had on

350   these lipid classes (**Figure 6D**). Overall, these data demonstrated that SOD2 deletion in

351   skeletal muscle impacts on specific lipid pathways that are an important energy source for the

352   mitochondria (i.e. FFAs). Moreover, there appeared to be a global impact on the level of

353   phospholipids, with a potential activation of the pathways that clear the more toxic

354   lysophospholipids such as LPC, LPE and LPI, into their acylated stable forms including PC

355   and PE, a process catalyzed by lysophosphatidylcholine acyltransferase (LPCAT). In

356   addition, an intriguing observation from these datasets is that the pathway responsible for

357   conversion of phosphatidic acid (PA) into diacylglycerol (DG), appeared to be substantially

358   impacted. This was evidenced by an increase in PA (the precursor) abundance and a decrease

359   in DG (the downstream product) abundance, a reaction that is catalyzed by the enzyme

360   phosphatidic acid phosphatase (PAP)/Lipin1. In light of these findings, we were interested to

361   investigate whether we could detect differences in the amount Lipin1 in skeletal muscle of

362   these animals. Western blotting for Lipin1 in WT and SOD2 KO muscles demonstrated that

363   there were no alterations in the overall abundance of Lipin1 between WT and KO muscles, in

364   either chow or HFD fed mice (**Figure 6E**). Collectively, these findings suggest that SOD2

15

365   either directly or indirectly affects pathways that are involved in the metabolism of lipids,

366   particularly phosphatidylcholine, providing interesting insights into a previously unexplored

367   role of SOD2 in skeletal muscle.

368 **Discussion**

369 In the current study, we demonstrate that post-developmental, skeletal muscle specific

370 deletion of SOD2 imparts subtle effects on whole body physiology, which likely manifest as

371 escalating deficits in mitochondrial function and subsequently energy metabolism. We also

372 identify previously unrecognised alterations in specific lipid pathways in SOD2 KO muscles,

373 which potentially define a new area of interest in the SOD2 field.

374

375 Previous studies investigating SOD2 deletion in skeletal muscle have done so either in

376 heterozygous global null models[12], or in muscle specific KO models that delete SOD2 whilst

377 the muscles are still developing in utero[14,15]. Our study is the first to our knowledge that

378 describes a deletion of SOD2 in skeletal muscle of mice that were already fully developed

379 (i.e. at 8 weeks of age). Subsequent deletion of SOD2 for approximately 14 weeks (almost

380 60% of their entire life), did not recapitulate much of the prior phenotypes related to SOD2

381 deficiency in skeletal muscle, identifying important caveats to previous literature. The failure

382 for our post-developmental model to recapitulate the robust muscle atrophy/weakness

383 phenotype and impairments in glucose metabolism described in previous studies, speaks to

384 the potential important roles of SOD2 in the developing muscle. Even when challenged with

385 a high fat-diet (HFD), which we demonstrated to drive increases in oxidative damage and

386 glucose intolerance, SOD2 KO mice did not demonstrate any additional deterioration.

387

388 Instead, the SOD2 KO mice demonstrated a more subtle phenotype, which, upon further

389 investigation revealed a hereto unrecognised link between SOD2 and lipid metabolism. This

390 included altered phospholipid (PL) abundance and the availability of important lipid

391 intermediates such as diacylglyerols (DG) and free fatty acids (FFA). It is plausible that these

392 pathways may have also been altered in previous models of SOD2 deletion, however it would

17

393 have been difficult to tease out these subtle effects from the well progressed and

394 overwhelming atrophy phenotype in those developmental models.

395

396 The alteration in these specific lipid species is intriguing, given that they all form part of a

397 larger signaling network that regulates metabolism and several other important systems in

398 skeletal muscle. Central to this network is the reciprocal regulation of phosphatidic acid (PA)

399 and DG abundance, which is facilitated by opposing actions of PAP/lipin1 (PA → DG) and

400 diacylglycerol kinase (DGK) (DG → PA)[22]. Several studies have investigated these specific

401 enzyme complexes in skeletal muscle, all of which have demonstrated consistent phenotypes

402 with that described in our and other muscle-specific SOD2 deletion studies. The data

403 presented in our current study, would suggest that loss of SOD2 in skeletal muscle leads to

404 either a reduction in PAP/Lipin1 activity, an increase in DGK activity, or a combination of

405 both. Indeed, Lipin1 deficiency in skeletal muscle, which increases PA abundance and

406 decreases DG abundance, leads to muscle atrophy, impaired autophagy and reductions in

407 mitochondrial function[23-25]. This is consistent with the lipid alterations and reductions in

408 mitochondrial protein abundance observed in SOD2 KO muscles. However, our data

409 demonstrate that Lipin1 levels were not altered by SOD2 KO, which may indicate a lack of

410 effect of this pathway. A caveat to these findings is that total abundance of Lipin1 is not a

411 robust readout of activity, and thus other measures of function such as phosphorylation would

412 strengthen these interpretations.

413

414 With regards to DGK, loss of different isoforms in skeletal muscle appears to impact on

415 insulin signaling and AMP kinase activity, but not on mitochondrial function. Specifically,

416 deletion of DGKδ increases DG levels, which in turn reduces AMPK phosphorylation and

417 impaired lipid oxidation[26]. In SOD2 KO muscles, we observed decreased DG abundance and

18

418   increased AMPK phosphorylation (in chow fed mice), consistent with effects described for

419   DGK pathways. Unfortunately, we do not have data on DGK activity, so we cannot comment

420   as to whether these pathways are responsible. Nevertheless, we speculate that in developed

421   skeletal muscle, deletion of SOD2 initially impacts on this PA/DG lipid axis, which

422   subsequently leads to reductions in mitochondrial function and a worsening lethargy

423   phenotype, further perpetuating the effect of SOD2 deletion.

424

425   Further support for this PA/DG pathway being instrumental to the SOD2 phenotype, comes

426   from studies performed in drosophila and *C. elegans*. Lin et al. described alterations in the

427   DG/PA pathway that impacted on longevity via the ability of PA to activate the mTOR

428   pathway[27]. These studies also demonstrated that modulation of these pathways resulted in

429   higher susceptibility to oxidative stress-induced alterations in lifespan. Thus, PA/DG and

430   oxidative stress may combine to form a critical axis that regulates skeletal muscle health and

431   lifespan.

432

433   Despite these several lines of evidence, it remains unknown how the loss of SOD2 impacts on

434   this axis, and perhaps disruption of redox signaling in skeletal muscle could influence PA

435   levels and enzymes important in these pathways. Recent studies from Neufer et al. (2020)

436   have demonstrated this to be a possibility, with studies from their lab linking beta-oxidation

437   and redox homeostasis with Lipin1 activity and insulin resistance[28,29]. It is also possible that

438   these proteins somehow interact with each other or within similar complexes, which might

439   alter their activity or substrate availability. However, preliminary investigations from our

440   group using deposited open-access protein-protein interaction datasets do not support this

441   hypothesis (not shown), with no evidence for a direct or secondary interaction between these

442   proteins. Another possibility is that loss of SOD2 subtly alters respiratory kinetics locally at

19

443   the mitochondrial membrane, which secondarily impacts substrate and lipidome abundance

444   within the mitochondria, leading to noticeable effects on cellular function over time. A recent

445   study demonstrated that skeletal muscle specific loss of the enzyme Phosphatidylserine

446   Decarboxylase (PSD), which synthesizes mitochondrial phosphatidylethaloamines (PE),

447   leads to striking defects in mitochondrial and muscle function[30]. This loss of PE resulted in

448   increased production of ROS from the mitochondria, implicating ROS as being important to

449   this phenotype. Although we do not observe alterations in PE levels in this model, these data

450   provide a direct role for mitochondrial lipids in regulating respiratory efficiency.

451

452   Overall, our data provide previously unrecognized effects of SOD2 deletion in skeletal

453   muscle. Whilst our whole body analyses demonstrate only moderate impacts of post-

454   developmental deletion of SOD2 on some aspects of metabolism and muscle function

455   compared to previous literature, our lipidomics analysis revealed intriguing alterations to the

456   PA/DG pathway - providing a new link between redox biology and mitochondrial function.

457   An obvious limitation to our current study is the short time frame over which we studied the

458   animals, and had we allowed the animals to age for a longer period, a more robust phenotype

459   may have developed. Moreover, we only challenged the animals with a HFD and no other

460   interventions such as intense exercise training or muscle strain. Indeed, the HFD may not

461   have been sufficient to precipitate the appropriate stress to accelerate disease. Conversely,

462   had we utilized a more accelerated disease model, we may not have observed some of the

463   subtle effects on lipid metabolism. Nevertheless, our current data provide unique insights into

464   the underlying mechanisms by which SOD2 functions in skeletal muscle, highlighting

465   previously unexplored interactions with specific lipid pathways important in development

466   and disease.

467 **Methods**

468 **Animals**

469 All animal experiments were approved by the Alfred Research Alliance (ARA) Animal

470 Ethics committee (E/1618/2016/B) and performed in accordance with the research guidelines

471 set out by the National Health and Medical Research Council of Australia. SOD2 deletion

472 was achieved using the Cre-Lox system. For inducible, skeletal muscle specific ablation,

473 SOD2 floxed mice (C57BL/6J, a kind gift from Prof Takahiko Shimizu, Chiba University,

474 Japan) were crossed with ACTA1-creERT2 mice (C57BL/6J background, Jackson

475 Laboratories) to generate male cohorts of SOD2$^{fl/fl}$-ACTA1-creERT2$^{+/-}$ (SOD2 mCre) or

476 SOD2$^{fl/fl}$-ACTA1-creERT2$^{-/-}$ (SOD2 WT). All mice were bred and sourced through the ARA

477 Precinct Animal Centre and randomly allocated to groups. Cohorts of SOD2 mCre and WT

478 mice were aged to 6-8 weeks of age before receiving oral gavage for 3 consecutive days of

479 either Tamoxifen (80mg/kg) in sunflower oil, or sunflower oil alone. Following gavage, mice

480 were left to recover for 2 weeks before being placed on high fat diet (43% energy from fat,

481 #SF04-001 Specialty Feeds) for 12 weeks, or remained on normal chow diet (normal rodent

482 chow, Specialty Feeds, Australia). Animals were housed at 22°C on a 12hr light/dark cycle

483 with access to food and water *ad libitum* with cages changed weekly. At the end of the study

484 mice were fasted for 4-6 hours and then anesthetized with a lethal dose of ketamine/xylazine

485 before blood and tissues were collected, weighed and frozen for subsequent analysis.

486

487 **Tissue Sections and Nitrotyrosine Immunohistochemistry**

488 TA muscles were carefully dissected and cut cross sectionally through the widest part of the

489 muscle tissue. One half of the TA was embedded cut side down in OCT before being frozen

490 in a bath of isopentane submerged in liquid nitrogen vapour. After freezing, blocks were

491 brought to -20°C and 5μm sections were cut using a Leica Cryostat and then subjected to

492   immunohistochemical staining for nitrotyrosine as described previously[31]. Briefly, mounted

493   sections of TA muscle were fixed with cold acetone, and endogenous peroxidases were

494   inactivated with 3% H_2O_2 in Tris-buffered saline. Sections were pre-blocked with a biotin-

495   avidin blocking kit (Vector Laboratories) and then incubated with the nitrotyrosine antibody

496   (Merck Milipore; 1:200) overnight at 4°C. Subsequent secondary antibody, biotinylated anti-

497   rabbit immunoglobulin 1:100 (Dako) was added for 30 min, followed by horseradish

498   peroxidase–conjugated streptavidin, diluted 1:500 (Dako), and incubated for 30 min in 3,3'-

499   diaminobenzidine tetrahydrochloride (DAB) (Sigma-Aldrich). Images were captured on an

500   Olympus Slide scanner VS120 (Olympus) and viewed in OlyVIA (Olympus, build 13771)

501   and quantitated using a singular threshold setting in Fiji across all samples[32].

502

503   **Peroxide Abundance using Amplex Red Assay**

504   Muscle peroxide abundance was determined using the Amplex Red assay, as previously

505   described[33]. Briefly, TA muscle tissue was homogenised using 20mM HEPES buffer

506   (containing 1mM EGTA, 210mM Mannitiol and 70mM sucrose). After normalising protein

507   concentration using a BCA assay (Pierce BCA assay kit), the quantification of hydrogen

508   peroxide was determined using the Amplex Red Hydrogen Peroxide/Peroxidase Assay Kit

509   (Molecular Probes) as per the manufacturer's instructions.

510

511   **Glucose Tolerance Tests**

512   Oral glucose tolerance tests (oGTT) were performed at different time points (0, 4 and 12

513   weeks post-HFD) throughout the study period at a dose of 1.5g/kg lean mass as determined

514   by EchoMRI. All oGTTs were performed after a 5 hour fast as previously described[34].

515

516   **EchoMRI**

517 Body composition was analysed using the 4-in1 NMR Body Composition Analyzer for Live

518 Small Animals, according to the recommendations of the manufacturer (EchoMRI LLC,

519 Houston, TX, USA). This provides measurements of lean mass, fat mass and free water in

520 living animals as previously described[34].

521

Whole Body Energetics

523 Mice were placed in the Promethion High-Definition Behavioral Phenotyping System for

524 Mice (Sable Systems International, North Las Vegas, NV, USA) at 2 weeks post-tamoxifen

525 (baseline) and 13 weeks post-Tamoxifen (11 weeks post HFD) of age for 3 consecutive days.

526 Recordings for respirometry including energy expenditure (EE) and respiratory exchange

527 ratio (RER) were collected over the final 24-hour period.

528

Movement and Probability Mapping using Promethion

530 Behavioural phenotyping was conducted using assessments of activity monitoring (X, Y, Z

531 beam breaks and wheel revolutions), in combination with food and water intake. The

532 Promethion EthoScan utility created time and locomotion budgets with behavioural transition

533 matrices for advanced behaviour analysis. Markov chain behaviour transition probability

534 matrices were visualised utilising agl (Automatic Graph Layout, Microsoft Research;

535 https://rise4fun.com/Agl/). Positional probability maps were generated across as an average

536 of all positional locations during the 24-hour data collection period. Data was analysed and

537 visualised in R (v3.5.3) with custom R scripts using the open-source SableBase package

538 (Thomas Forester, 2016, Sable Systems International, Las Vegas, version 1.0).

539

SDS-PAGE and Immunoblot

23

541   Skeletal muscle was lysed in radio-immunoprecipitation assay (RIPA) buffer supplemented

542   with protease and phosphatase inhibitors. Matched protein quantities were separated by SDS-

543   PAGE and transferred to PVDF membranes. Membranes were blocked in 3% skim milk for 2

544   hours and then incubated with primary antibody overnight at 4°C for the following proteins:

545   4HNE (Abcam, ab46545), β-actin (Santa Cruz Biotech), Total OXPHOS Rodent WB

546   Antibody Cocktail (MitoSciences), pan 14-3-3 (Santa Cruz), phospho-T172 AMPKalpha

547   (Cell Signaling), Lipin-1 (Santa-Cruz Biotech) and total AMPKalpha (Cell Signaling). After

548   incubation with primary antibodies, membranes were washed and probed with their

549   respective HRP-conjugate secondary anti mouse or anti rabbit (Biorad) antibodies in 3% skim

550   milk for 2 hours at room temperature, then visualised with enhanced chemiluminescent

551   substrate (Pierce). Approximated molecular weights of proteins were determined from a co-

552   resolved molecular weight standard (BioRad, #1610374). Image Lab Software (Bio-Rad) was

553   used to perform densitometry analyses, and all quantification results were normalised to their

554   respective loading control or total protein.

555

556   **Quantitative PCR (qPCR)**

557   RNA was isolated from TA, EDL and Soleus muscles using RNAzol reagent and isopropanol

558   precipitation. cDNA was generated from RNA using MMLV reverse transcriptase

559   (Invitrogen) according to the manufacturer's instructions. qPCR was performed on 10ng of

560   cDNA using the SYBR-green method on a QuantStudio 7 Flex Real-Time PCR System,

561   using primer sets outlined in Table 1. Primers were designed to span exon-exon junctions

562   where possible, and were tested for specificity using BLAST (Basic Local Alignment Search

563   Tool; National Centre for Biotechnology Information). Amplification of a single amplicon

564   was estimated from melt curve analysis, ensuring only a single peak and an expected

565   temperature dissociation profile were observed. Quantification of a given gene was

24

566 determined by the relative mRNA level compared with control using the delta-CT method,

567 which was calculated after normalisation to the housekeeping gene *Ppia* or *Rplp0*.

568

569 **Mitochondrial (mt)DNA to nuclear (n)DNA ratio**

570 TA muscle tissue was homogenised in digestion buffer (100mM NaCl, 10mM Tris-HCl,

571 25mM EDTA, 0.5% SDS, pH 8.0) and then incubated in Proteinase K (250U/mL) for 1 hour

572 at 55°C. Following this, total DNA was isolated using the phenol-chloroform extraction

573 method. A qPCR reaction was then performed on 5ng of total DNA using a primer set that

574 amplifies the mitochondrial gene mtCO3, and the genomic gene SDHA (see table 1 for

575 primer sequences). Estimated abundance of each gene was used to generate a ratio of

576 mitochondrial to nuclear DNA (mtDNA/nDNA), and this ratio was compared between

577 genotypes.

578

579 **Lipidomics**

580 Lipidomics was performed on approximately 50µg of soluble protein (homogenised and

581 sonicated) from TA muscles taken from SOD2 WT+OIL, mCre+OIL, WT+TAM and

582 mCre+TAM using LC electrospray ionisation MS/MS (LC-ESI-MS/MS) on an Agilent 6490

583 triple quadrupole (QQQ) mass spectrometer coupled with an Agilent 1290 series HPLC

584 system and a ZORBAX eclipse plus C18 column as previously described[35].

585

586 **Statistical Analyses**

587 All data were expressed as mean ± standard error of the mean (SEM), except where otherwise

588 stated (i.e. Figure 6A). Statistical comparisons in animal studies were analyzed by repeated

589 measures 2-way ANOVA, two-way ANOVA with post-hoc testing, or one-way ANOVA

590 with po-hoc testing as indicated in figure legends. Lipidomics, tissue analysis and cell based

591 experiments were analyzed by either ANOVA with post-hoc testing (Fishers LSD) where

592 appropriate, or paired students' t-test unless otherwise stated. Analyses were performed using

593 PRISM8 software and a p-value of $p < 0.05$ was considered statistically significant.

594

595 **Data Inclusion and Exclusion Criteria**

596 For animal experiments, phenotyping data points were excluded using pre-determined criteria

597 if the animal was unwell at the time of analysis, there were technical issues identified (such

598 as failed data acquisition in Promethion), values were biological implausible (such as

599 RER=2.0) or data points that were identified as outliers using Tukey's Outlier Detection

600 Method (1.5IQR below Q1 or 1.5IQR above Q3). If repeated data points from the same

601 mouse failed QC based on pre-determined criteria, or several data points were outliers as per

602 Tukey's rule, the entire animal was excluded from that given analysis (i.e. during glucose

603 tolerance tests, indicating inaccurate dosing with gavage). For in vivo and in vitro tissue and

604 molecular analysis, data points were only excluded if there was a technical failure (i.e. poor

605 RNA quality, failed amplification in qPCR, failed injection in mass spectrometer), or the

606 value was biological improbable. This was performed in a blinded fashion (i.e. on grouped

607 datasets before genotypes were known).

608

609   **Tables**

Gene	Forward primer (5' – 3')	Reverse primer (5' – 3')
Nrf2	CATGATGGACTTGGAGTTGC	CCTCCAAAGGATGTCAATCAA
Ncf1	CCGGCTATTTCCCATCCAT	TCGCTGGGCCTGGGTTAT
Cyba	AGATCGAGTGGGCCATG	CTTGGGTTTAGGCTCAAT
Nox2	AGTGCGTGTTGCTCGACAAG	CCAAGCTACCATCTTATGGAAAGTG
Cre	AGGGCGCGAGTTGATAGCT	GAGCGATGGATTTCCGTCTCT
Sod2	AGGCTCTGGCCAAGGGAGAT	CACGCTTGATAGCCTCCAGCA
Tfeb	GGAGCCAGAGCTGCTTGTTA	AACAAAGGCACCATCCTCAA
Polg1	TAGCTGGCTGGTCCAAGAGT	CGACGTGGAGGTCTGCTT
Cytc	CAGCTTCCATTGCGGACAC	CGCTGACAGCATCACCTTTC
Tfam	AGCTTGTAAATGAGGCTTGGA	AGATGTCTCCGGATCGTTTC
Ndufs1	CACTCGTTCCACCTCAGCTA	GACGGCTCCTCTACTGCCT
Ppargc1a	TGAGGACCGCTAGCAAGTTT	TGAAGTGGTGTAGCGACCAA
Got2	ATGGCTGCTGCCTTTCAC	GATCTGGAGGTCCCATTTCA
Hk2	GGAACCGCCTAGAAATCTCC	GGAGCTCAACCAAAACCAAG
Glut1	GGTGTGCAGCAGCCTGTGT	CACAGTGAAGGCCGTGTTGA
Cpt1a	GACTCCGCTCGCTCATTC	TCTGCCATCTTGAGTGGTGA
Cpt1b	CATCCCAGGCAAAGAGACA	AAGCGACCTTTGTGGTAGACA
Uvrag	TTGCACACTGGGCTCTATGA	TGAACACAAGGGTCATCCAA
Fgf21	AGATGGAGCTCTCTATGGATCG	GGGCTTCAGACTGGTACACAT
Vegfa	AATGCTTTCTCCGCTCTGAA	CTCACCAAAGCCAGCACATA
Mef2c	GCCGGACAAACTCAGACATTG	GGGTTTCCCAGTGTGCTGAC
Myog	CAACCAGGAGGAGCGCGATCTCCG	AGGCGCTGTGGGAGTTGCATTCACT
Myod	AGGCCGTGGCAGCGA	GCTGTAATCCATCATGCCATCA
Ppia	AGCCAAATCCTTTCTCTCCAG	CACCGTGTTCTTCGACATCA
Rplp0	ACCCTGAAGTGCTCGACATC	ATTGATGATGGAGTGTGGCA
Sdha*	TGGACCCATCTTCTATGC	TACTACAGCCCCAAGTCT
mtCO3*	GCAGGATTCTTCTGAGCGTTCT	GTCAGCAGCCTCCTAGATCATGT

610

611

612   **Table 1**

613   Forward and reverse primer sets for detection of the designated gene using qPCR. (m =

614   mouse). * indicates primer sets used on DNA, to determine the mtDNA/tDNA ratio.

615

623

624   **Author contributions**

625   BGD conceived and designed the study, and wrote the manuscript. BGD, AZ, CY, YL, YT,

626   STB, SW, TS performed all experiments. AS and JBdeH performed and analysed Amplex

627   Red and Nitrotyrosine assays. PJM provided expertise in lipidomics analysis. MTC provided

628   access to floxed mice and ongoing research support. ACC provided reagents, experimental

629   advice and access to resources. All authors read and approved the manuscript.

630

631   **Conflicts of interest**

632   The authors declare that they have no conflicts of interest.

633

634

28

References

635

636   1.   Wanagat, J. & Hevener, A.L. Mitochondrial quality control in insulin resistance and

637   diabetes. *Curr Opin Genet Dev* **38**, 118-126 (2016).

638   2.   Montgomery, M.K. & Turner, N. Mitochondrial dysfunction and insulin resistance: an

639   update. *Endocrine connections* **4**, R1-R15 (2015).

640   3.   Trifunovic, A., *et al.* Premature ageing in mice expressing defective mitochondrial

641   DNA polymerase. *Nature* **429**, 417-423 (2004).

642   4.   Giacco, F. & Brownlee, M. Oxidative stress and diabetic complications. *Circ Res* **107**,

643   1058-1070 (2010).

644   5.   Brownlee, M. The pathobiology of diabetic complications: a unifying mechanism.

645   *Diabetes* **54**, 1615-1625 (2005).

646   6.   Kauppila, T.E.S., Kauppila, J.H.K. & Larsson, N.G. Mammalian Mitochondria and

647   Aging: An Update. *Cell metabolism* **25**, 57-71 (2017).

648   7.   Andreux, P.A., Houtkooper, R.H. & Auwerx, J. Pharmacological approaches to

649   restore mitochondrial function. *Nature reviews. Drug discovery* **12**, 465-483 (2013).

650   8.   Boden, M.J., *et al.* Overexpression of manganese superoxide dismutase ameliorates

651   high-fat diet-induced insulin resistance in rat skeletal muscle. *American journal of*

652   *physiology. Endocrinology and metabolism* **303**, E798-805 (2012).

653   9.   Hoehn, K.L., *et al.* Insulin resistance is a cellular antioxidant defense mechanism.

654   *Proceedings of the National Academy of Sciences of the United States of America*

655   **106**, 17787-17792 (2009).

656   10.   Li, Y., *et al.* Dilated cardiomyopathy and neonatal lethality in mutant mice lacking

657   manganese superoxide dismutase. *Nature genetics* **11**, 376-381 (1995).

658   11.   Crane, J.D., *et al.* Elevated mitochondrial oxidative stress impairs metabolic

659   adaptations to exercise in skeletal muscle. *PloS one* **8**, e81879 (2013).

660   12.   Kang, L., *et al.* Heterozygous SOD2 deletion impairs glucose-stimulated insulin

661   secretion, but not insulin action, in high-fat-fed mice. *Diabetes* **63**, 3699-3710 (2014).

662   13.   Koyama, H., *et al.* Antioxidants improve the phenotypes of dilated cardiomyopathy

663   and muscle fatigue in mitochondrial superoxide dismutase-deficient mice. *Molecules*

664   **18**, 1383-1393 (2013).

665   14.   Kuwahara, H., *et al.* Oxidative stress in skeletal muscle causes severe disturbance of

666   exercise activity without muscle atrophy. *Free radical biology & medicine* **48**, 1252-

667   1262 (2010).

668   15.   Lustgarten, M.S., *et al.* Conditional knockout of Mn-SOD targeted to type IIB skeletal

669   muscle fibers increases oxidative stress and is sufficient to alter aerobic exercise

670   capacity. *American journal of physiology. Cell physiology* **297**, C1520-1532 (2009).

671   16.   Ikegami, T., *et al.* Model mice for tissue-specific deletion of the manganese

672   superoxide dismutase (MnSOD) gene. *Biochemical and biophysical research*

673   *communications* **296**, 729-736 (2002).

674   17.   Izuo, N., *et al.* Brain-Specific Superoxide Dismutase 2 Deficiency Causes Perinatal

675   Death with Spongiform Encephalopathy in Mice. *Oxidative medicine and cellular*

676   *longevity* **2015**, 238914 (2015).

677   18.   Han, Y.H., *et al.* Adipocyte-Specific Deletion of Manganese Superoxide Dismutase

678   Protects From Diet-Induced Obesity Through Increased Mitochondrial Uncoupling

679   and Biogenesis. *Diabetes* **65**, 2639-2651 (2016).

680   19.   Kawakami, S., *et al.* Antioxidant, EUK-8, prevents murine dilated cardiomyopathy.

681   *Circulation journal : official journal of the Japanese Circulation Society* **73**, 2125-

682   2134 (2009).

683 20. Liu, G.*, et al.* Bladder function in mice with inducible smooth muscle-specific

684   deletion of the manganese superoxide dismutase gene. *American journal of*

685   *physiology. Cell physiology* **309**, C169-178 (2015).

686 21. Ahn, B.*, et al.* Mitochondrial oxidative stress impairs contractile function but

687   paradoxically increases muscle mass via fibre branching. *Journal of cachexia,*

688   *sarcopenia and muscle* **10**, 411-428 (2019).

689 22. Brindley, D.N., Pilquil, C., Sariahmetoglu, M. & Reue, K. Phosphatidate degradation:

690   phosphatidate phosphatases (lipins) and lipid phosphate phosphatases. *Biochimica et*

691   *biophysica acta* **1791**, 956-961 (2009).

692 23. Zhang, P., Verity, M.A. & Reue, K. Lipin-1 regulates autophagy clearance and

693   intersects with statin drug effects in skeletal muscle. *Cell metabolism* **20**, 267-279

694   (2014).

695 24. Schweitzer, G.G.*, et al.* Loss of lipin 1-mediated phosphatidic acid phosphohydrolase

696   activity in muscle leads to skeletal myopathy in mice. *FASEB journal : official*

697   *publication of the Federation of American Societies for Experimental Biology* **33**,

698   652-667 (2019).

699 25. Rashid, T.*, et al.* Lipin1 deficiency causes sarcoplasmic reticulum stress and

700   chaperone-responsive myopathy. *The EMBO journal* **38**(2019).

701 26. Jiang, L.Q.*, et al.* Diacylglycerol kinase-delta regulates AMPK signaling, lipid

702   metabolism, and skeletal muscle energetics. *American journal of physiology.*

703   *Endocrinology and metabolism* **310**, E51-60 (2016).

704 27. Lin, Y.H.*, et al.* Diacylglycerol lipase regulates lifespan and oxidative stress response

705   by inversely modulating TOR signaling in Drosophila and C. elegans. *Aging cell* **13**,

706   755-764 (2014).

31

707   28.   Smith, C.D., Schmidt, C.A., Lin, C.T., Fisher-Wellman, K.H. & Neufer, P.D. Flux

708   through mitochondrial redox circuits linked to nicotinamide nucleotide

709   transhydrogenase generates counterbalance changes in energy expenditure. *The*

710   *Journal of biological chemistry* **295**, 16207-16216 (2020).

711   29.   Smith, C.D.*, et al.* Genetically increasing flux through beta-oxidation in skeletal

712   muscle increases mitochondrial reductive stress and glucose intolerance. *American*

713   *journal of physiology. Endocrinology and metabolism* (2021).

714   30.   Heden, T.D.*, et al.* Mitochondrial PE potentiates respiratory enzymes to amplify

715   skeletal muscle aerobic capacity. *Science advances* **5**, eaax8352 (2019).

716   31.   Sharma, A.*, et al.* Direct Endothelial Nitric Oxide Synthase Activation Provides

717   Atheroprotection in Diabetes-Accelerated Atherosclerosis. *Diabetes* **64**, 3937-3950

718   (2015).

719   32.   Schindelin, J.*, et al.* Fiji: an open-source platform for biological-image analysis. *Nat*

720   *Methods* **9**, 676-682 (2012).

721   33.   Sharma, A.*, et al.* The nuclear factor (erythroid-derived 2)-like 2 (Nrf2) activator

722   dh404 protects against diabetes-induced endothelial dysfunction. *Cardiovasc Diabetol*

723   **16**, 33 (2017).

724   34.   Bond, S.T., Kim, J., Calkin, A.C. & Drew, B.G. The Antioxidant Moiety of MitoQ

725   Imparts Minimal Metabolic Effects in Adipose Tissue of High Fat Fed Mice.

726   *Frontiers in physiology* **10**, 543 (2019).

727   35.   Huynh, K.*, et al.* High-Throughput Plasma Lipidomics: Detailed Mapping of the

728   Associations with Cardiometabolic Risk Factors. *Cell chemical biology* **26**, 71-84 e74

729   (2019).

730

731

732   **Figure Legends**

733

734   **Figure 1: Generation and characterisation of inducible, skeletal muscle specific SOD2**

735   **knock out mice.** mRNA expression of **(A)** cre recombinase and **(B)** SOD2 in liver, white

736   adipose tissue (WAT) and TA muscle of SOD2 WT and mCre mice (n=4/group); **(C)** Cre

737   recombinase and **(D)** SOD2 mRNA expression across three different muscle types (TA,

738   Soleus and EDL) of WT and mCre positive mice (n=6-11/group); **(E)** Western blots for

739   SOD2 and β-actin in TA muscle lysates from WT plus tamoxifen (WT) and mCre plus

740   tamoxifen (KO) mice fed either a chow or high fat diet (HFD; n=3-4/group). mRNA

741   expression of redox genes from **(F)** TA, **(G)** EDL and **(H)** soleus muscles from the four HFD

742   fed cohorts (n=4-11/group); **(I)** Western blot and **(J)** quantitation of 4-hydroxynonenal

743   (4HNE) conjugated proteins from TA of WT plus tamoxifen (WT) and mCre plus tamoxifen

744   (KO) mice fed either a chow or HFD (n=3-4/group); **(K)** Skeletal muscle peroxide abundance

745   as determined by Amplex Red assay in TA muscles from WT and KO chow fed mice and

746   WT+OIL, mCre+OIL, WT+TAM, mCre+TAM cohorts fed a chow or HFD (n=3-10/group);

747   **(L)** Quantification of Nitrotyrosine staining as determined by immunohistochemistry

748   performed on sections of TA muscles from WT+TAM and mCre+TAM fed a HFD (n=7-

749   10/group) All data are presented as mean ± SEM. Data with >2 groups were compared by

750   ANOVA with Fishers LSD post-hoc testing, samples with 2 groups were analysed using a

751   Mann-Whitney non-parametric t-test where * denotes a p-value<0.05. WAT = white adipose

752   tissue, TA = *Tibialis anterior*, EDL = *Extensor digitorum longus*, 4HNE = 4-hydroxynonenal

753   , DAB = 3,3'-Diaminobenzidine; HFD = high fat diet.

754

755   **Figure 2: General features and tissue weights of inducible, skeletal muscle specific KO**

756   **mice. (A)** Weekly total body weight of the four cohorts fed a HFD for 12 weeks (n=4-

757   11/group); **(B)** Lean mass and **(C)** fat mass as determined by EchoMRI in the four HFD fed

758   cohorts at baseline, 4 weeks, 8 weeks and 12 weeks post-HFD (n=4-11/group); Tissue weight

759   for **(D)** EDL, **(E)** TA, **(F)** liver and **(G)** gonadal WAT (gWAT) normalized to body weight

760   (BW) at study end (n=4-11/group). Data are presented as mean ± SEM. Data in (A-C) were

761   analysed using repeated measures two-way ANOVA. All other data were compared by

762   ANOVA with Fishers LSD post-hoc testing. g = grams, mg = milligrams, wks = weeks, HFD

763   = high fat diet, TA = *Tibialis anterior*, EDL = *Extensor digitorum longus*, gWAT = gonadal

764   white adipose tissue, BW = body weight.

765

766   **Figure 3: Measurements of whole body metabolism and glucose tolerance in inducible,**

767   **muscle specific SOD2 KO mice. (A)** Respiratory exchange ratio (RER) trace from

768   Promethion analysis over the entire 24 hour assessment period, **(B)** average RER and **(C)**

769   average energy expenditure (EE) for WT+TAM (light blue) and mCRE+TAM (dark blue)

770   mice in the light and dark periods; **(D)** Average RER and **(E)** average energy expenditure

771   (EE) for both genotypes in the light and dark periods prior to study end; **(F)** Total locomoter

772   activity (pedal and wheel movement) over the 24 hour assessment period at the end of the

773   HFD feeding study; Change in **(G)** average wheel distance and **(H)** average wheel speed

774   from baseline to study end during the light and dark cycles; Locality mapping of mice based

775   on 24 hours of movement data during the **(I)** light cycle (day time) and **(J)** dark cycle (night

776   time). Map colours indicate increasing time spent in that given location (red being most,

777   yellow being least). Intense red areas indicate "lounge spots", likely representing regions

778   where mice spent time resting for longer periods. Grey boxes designate each fixed cage

779   component (i.e. wheel, food hopper, water sipper and running wheel). Probability mapping

780   for **(K)** WT+TAM mice and **(L)** mCRE+TAM mice estimates predicted behavior

781   (percentage) following a certain activity. Red numbers indicate an increase, whilst blue
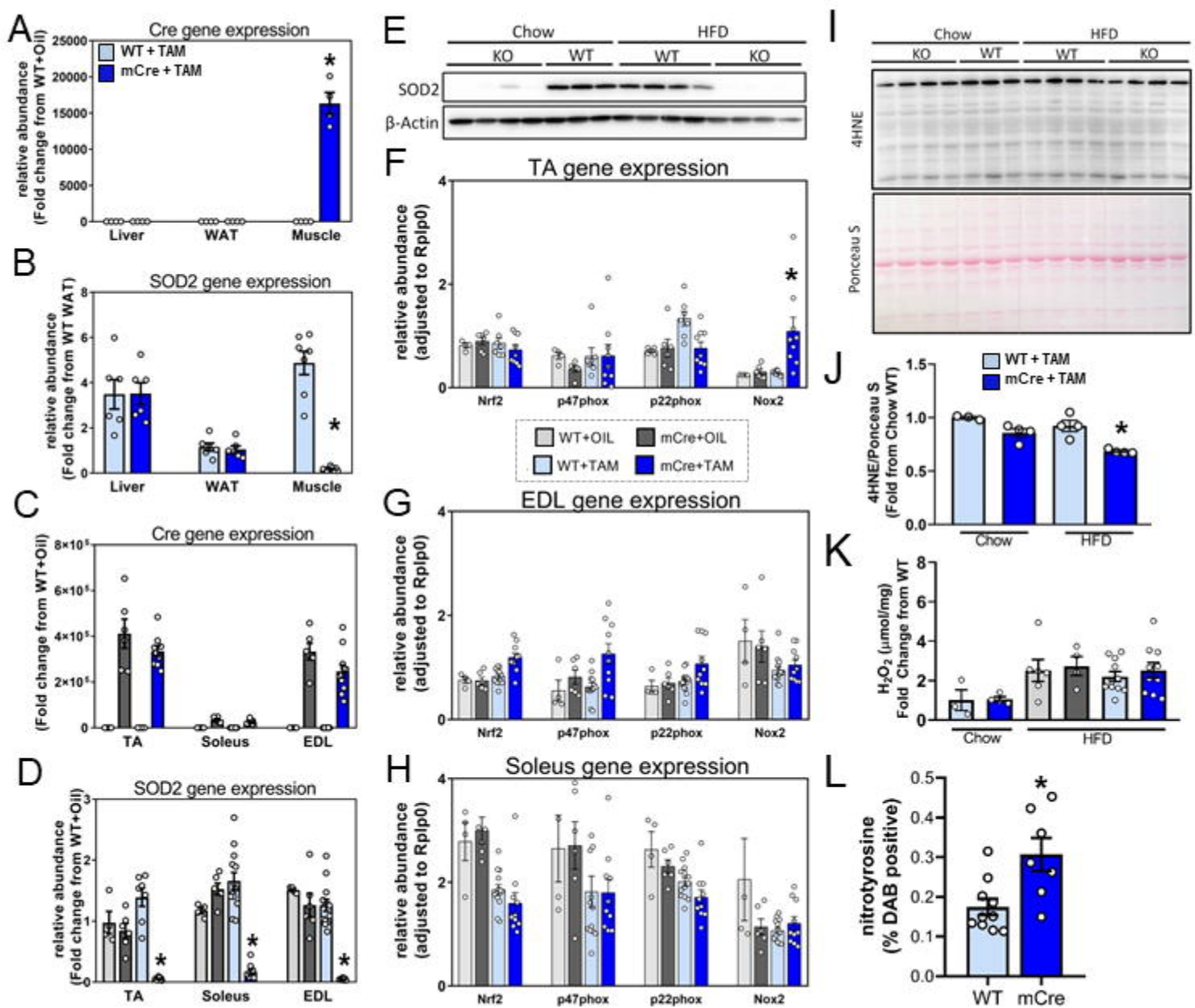
34

782   numbers indicate a decrease in that behavior in KO mice relative to WT mice, *slnge* = short

783   lounge, *llnge* = long lounge. Fasting blood glucose (FBG) measurement and oral glucose

784   tolerance tests (oGTT) in mice at **(M, N)** baseline, **(O, P)** 4 weeks post-HFD and **(Q, R)** 12

785   weeks post-HFD respectively. Data are presented as mean ± SEM (B-E, G, H, M-R). Data in

786   (N, P and R) were compared using repeated measures ANOVA. All other data were

787   compared by ANOVA with Fishers LSD post-hoc testing where * indicates a p-value<0.05.

788   RER = respiratory exchange ratio, EE = energy expenditure, HFD = high fat diet.

789

790   **Figure 4: Analysis of mitochondrial abundance and gene expression in muscles from**

791   **inducible, skeletal muscle specific SOD2 KO mice. (A)** Mitochondrial DNA (mtDNA) to

792   nuclear DNA (nDNA) ratio in TA muscles of the four HFD fed cohorts; **(B)** Western blot on

793   protein from TA muscles isolated from WT+TAM (WT) and mCre+TAM (KO) mice fed a

794   chow diet or high fat diet (HFD) for proteins from the 5 complexes (CI-CV) of the

795   mitochondrial electron transport chain (ETC) and of pan 14-3-3 (loading control). **(C)**

796   Quantification of five proteins from complexes of the ETC from panel B, normalized to the

797   the loading control (14-3-3); qPCR analysis for genes involved in skeletal muscle

798   mitochondrial function from **(D)** TA **(E)** EDL and **(F)** Soleus muscles from all four cohorts

799   of HFD fed mice. All data are presented as mean ± SEM. All data were compared by

800   ANOVA with Fishers LSD post-hoc testing where * indicates a p-value<0.05. TA = *Tibialis*
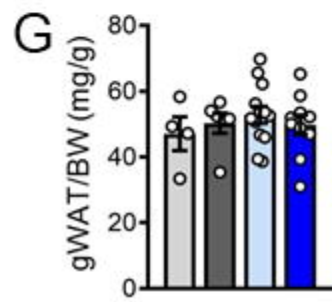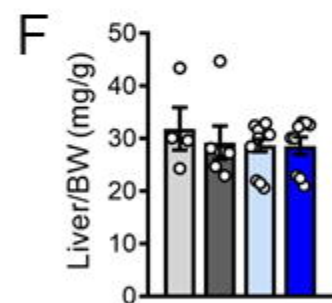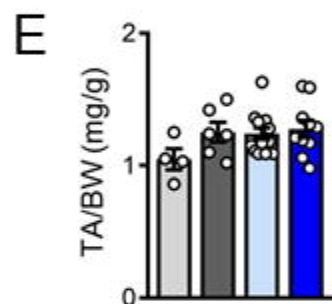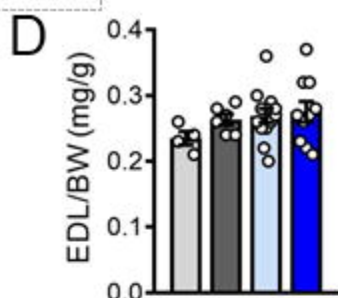
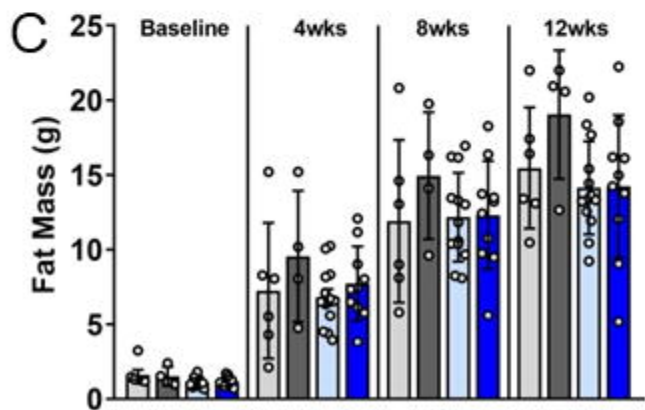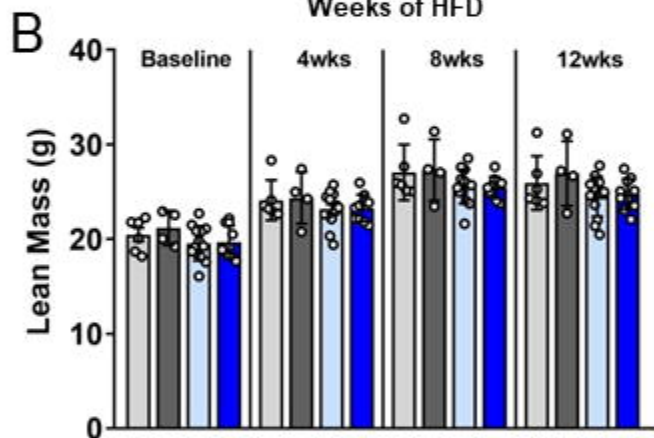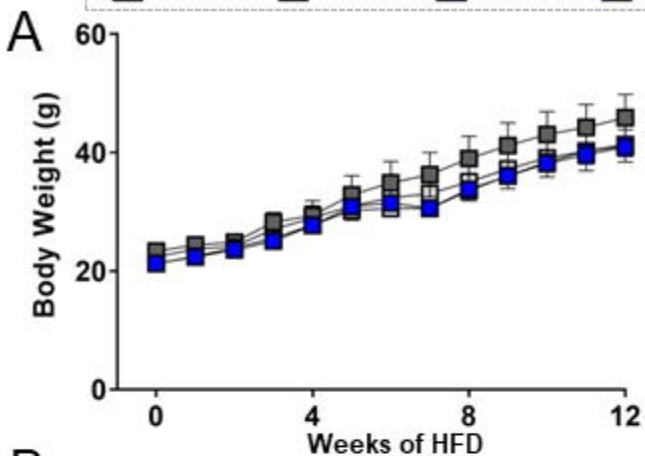801   *anterior*, EDL = *Extensor digitorum longus*.

802

803   **Figure 5: Analysis of AMP kinase activation and skeletal muscle gene expression in**

804   **muscles from inducible, skeletal muscle specific SOD2 KO mice.** (A) Western blot on

805   protein from TA muscles isolated from WT+TAM (WT) and mCre+TAM (KO) mice fed a

806   chow diet or HFD for phosphorylated AMP kinase (pAMPK T172), and total AMP kinase
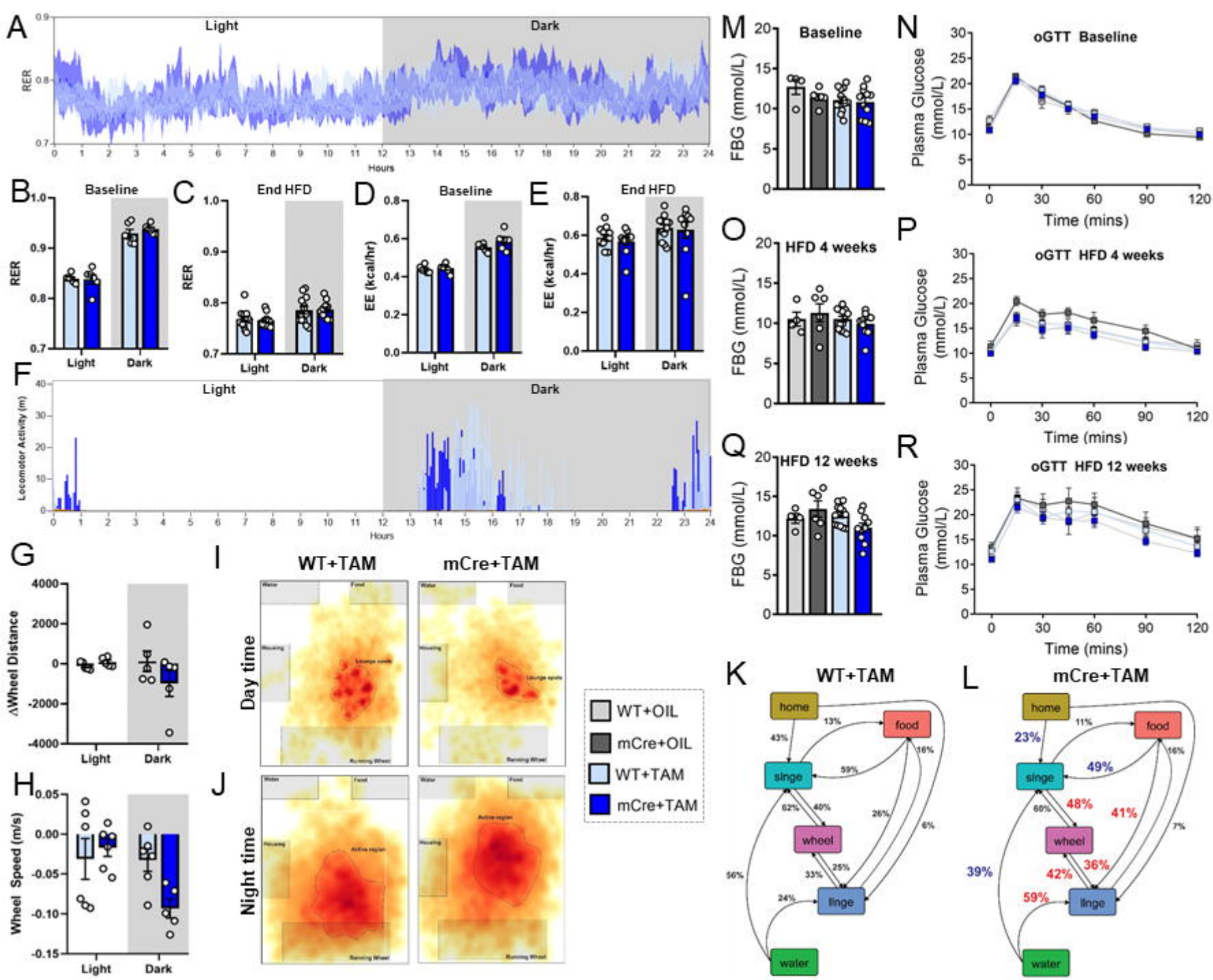
807   (tAMPK, loading control), and; (B) quantification of pAMPK/tAMPK abundance. qPCR

808   analysis for genes involved in skeletal muscle metabolism and function from (C) TA (D)

809   EDL and (E) soleus muscles from all four cohorts of HFD fed mice. Data presented as mean

810   ± SEM. All data were compared by ANOVA with Fishers LSD post-hoc testing where *

811   indicates a p-value<0.05. HFD = high fat diet, TA = *Tibialis anterior*, EDL = *Extensor*
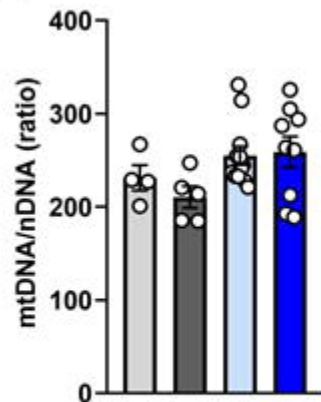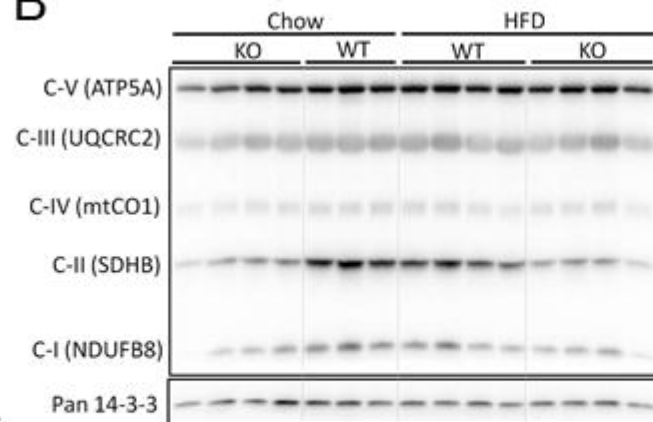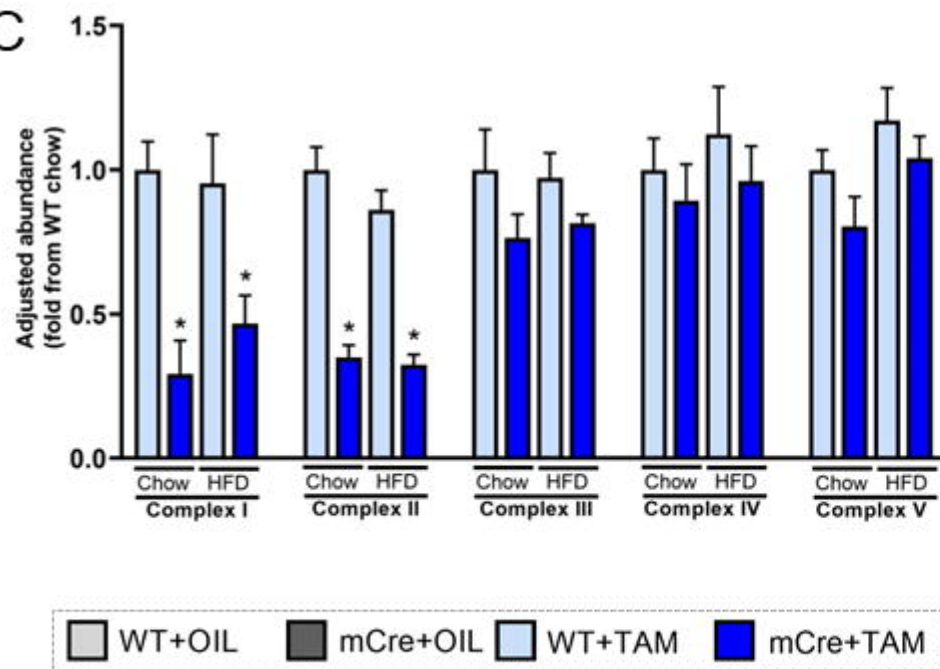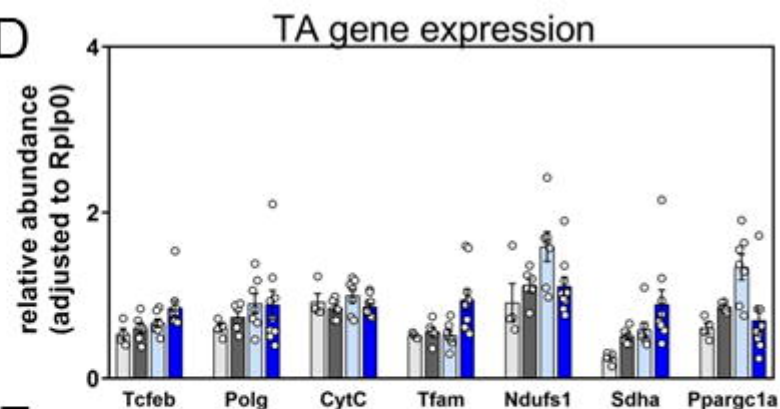
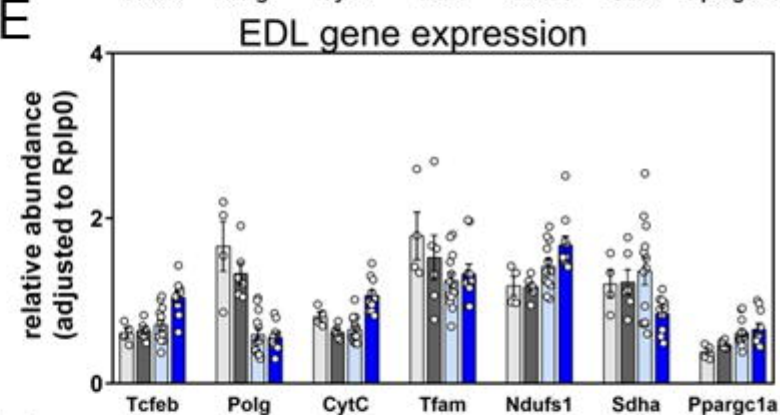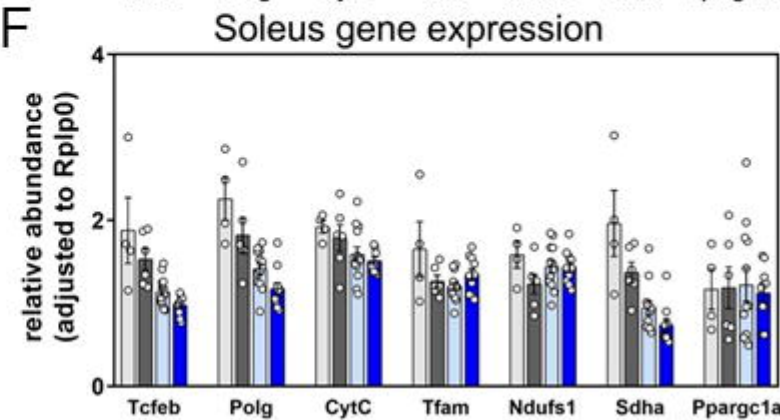812   *digitorum longus.*

813

814   **Figure 6: Analysis of lipid abundance in muscles from inducible, skeletal muscle specific**

815   **SOD2 KO mice.** Lipidomic assessment of lipid abundance in TA muscles from all four

816   cohorts of HFD fed mice. (A) Total abundance of the 33 classes of lipid quantified in TA

817   muscles across the four genotypes. Data are presented as $\log_2$ fold change from WT+TAM

818   samples using box and whisker plots with black line representing the median, boxes

819   representing the 25th and 75th percentile, whiskers represent 10-90th percentile whilst

820   individual dots represent values outside the 10th and 90th percentile. Heatmaps depicting

821   abundance (µmol/mg) of individual species of (B) diacylglycerol (DG), (C) fatty acids (FA)

822   and (D) total abundance of lysophosphatidylcholine (LPC), lysophosphatidylethanolamine

823   (LPE) and lysophosphatidylinositol (LPI) lipids in TA muscle. Crossed boxes indicate

824   species that were below the limit of detection. White boxes indicate species that fall below

825   the lowest unit in the scale. Scale represents red as the highest abundance and light blue as

826   the lowest abundance within a given range (shown on individual scale bars). (E) Western blot

827   on protein from TA muscles isolated from WT+TAM (WT) and mCre+TAM (KO) mice fed

828   a chow or high fat diet for Lipin1 and β-actin. Data in A-D were analysed by ANOVA with

829   Benjamini-Hochberg correction (applied per sub-analysis) where * indicates a p-value<0.05.

A Cre gene expression

B SOD2 gene expression

C Cre gene expression

D SOD2 gene expression

E

F TA gene expression

G EDL gene expression

H Soleus gene expression

I

J

K

L

WT + TAM
mCre + TAM

WT+OIL   mCre+OIL
WT+TAM   mCre+TAM

A — Light / Dark, RER over Hours (0–24)

B Baseline — RER (Light, Dark)

C End HFD — RER (Light, Dark)

D Baseline — EE (kcal/hr) (Light, Dark)

E End HFD — EE (kcal/hr) (Light, Dark)

F — Light / Dark, Locomotor Activity (m) over Hours

G — ΔWheel Distance (Light, Dark)

H — Wheel Speed (m/s) (Light, Dark)

I WT+TAM / mCre+TAM — Day time (Lounge spots)

J WT+TAM / mCre+TAM — Night time (Active region)

Legend:
- WT+OIL
- mCre+OIL
- WT+TAM
- mCre+TAM

M Baseline — FBG (mmol/L)

N oGTT Baseline — Plasma Glucose (mmol/L) vs Time (mins)

O HFD 4 weeks — FBG (mmol/L)

P oGTT HFD 4 weeks — Plasma Glucose (mmol/L) vs Time (mins)

Q HFD 12 weeks — FBG (mmol/L)

R oGTT HFD 12 weeks — Plasma Glucose (mmol/L) vs Time (mins)

K WT+TAM
- home → singe 43%, home → food 13%
- singe → food 59%, singe → wheel 40%, singe 62%
- food → 16%, → 26%, → 6%
- wheel → linge 25%, 33%
- linge → 24%, 56%
- water

L mCre+TAM
- home → singe 23%, home → food 11%
- singe → food 49%, singe → wheel 48%, singe 60%
- food → 16%, → 41%, → 7%
- wheel → linge 36%, 42%
- linge → 59%, 39%
- water

A pAMPK/tAMPK

B TA gene expression

C EDL gene expression

D Soleus gene expression

WT+OIL   mCre+OIL   WT+TAM   mCre+TAM